Int. J. Radiation Oncology Biol. Phys., Vol. 79, No. 1, pp. 269–278, 2011

0360-3016/$–see front matter

ELSEVIER

doi:10.1016/j.ijrobp.2010.02.052

PHYSICS CONTRIBUTION

REAL-TIME TARGET POSITION ESTIMATION USING STEREOSCOPIC KILOVOLTAGE/MEGAVOLTAGE IMAGING AND EXTERNAL RESPIRATORY MONITORING FOR DYNAMIC MULTILEAF COLLIMATOR TRACKING

BYUNGCHUL CHO, PH.D.,* PER RUGAARD POULSEN, PH.D.,*† AMIT SAWANT, PH.D.,* DAN RUAN, PH.D.,* AND PAUL J. KEALL, PH.D.*

*Department of Radiation Oncology, Stanford University, Stanford, CA; †Department of Medical Physics, Department of Radiation Oncology, Aarhus University, Aarhus, Denmark

Purpose: To develop a real-time target position estimation method using stereoscopic kilovoltage (kV)/megavoltage (MV) imaging and external respiratory monitoring, and to investigate the performance of a dynamic multileaf collimator tracking system using this method.

Methods and Materials: The real-time three-dimensional internal target position estimation was established by creating a time-varying correlation model that connected the external respiratory signals with the internal target motion measured intermittently using kV/MV imaging. The method was integrated into a dynamic multileaf collimator tracking system. Tracking experiments were performed for 10 thoracic/abdominal traces. A three-dimensional motion platform carrying a gold marker and a separate one-dimensional motion platform were used to reproduce the target and external respiratory motion, respectively. The target positions were detected by kV (1 Hz) and MV (5.2 Hz) imaging, and external respiratory motion was captured by an optical system (30 Hz). The beam–target alignment error was quantified as the positional difference between the target and circular beam center on the MV images acquired during tracking. The correlation model error was quantified by comparing a model estimate and measured target positions.

Results: The root-mean-square errors in the beam–target alignment that had ranged from 3.1 to 7.6 mm without tracking were reduced to <1.5 mm with tracking, except during the model building period (6 s). The root-mean-square error in the correlation model was submillimeters in all directions.

Conclusion: A novel real-time target position estimation method was developed and integrated into a dynamic multileaf collimator tracking system and demonstrated an average submillimeter geometric accuracy after initializing the internal/external correlation model. The method used hardware tools available on linear accelerators and therefore shows promise for clinical implementation.

Real-time tumor tracking, x-ray image guidance, external respiratory surrogate, respiratory tumor motion, dynamic multileaf collimator.

INTRODUCTION

Many linear accelerators have both gantry-mounted kilovoltage (kV) and megavoltage (MV) imaging systems that are actively being used for tumor localization and volumetric imaging but are not routinely used for tumor tracking. In an effort to use the imaging systems for intrafraction motion management of thoracic and abdominal tumors, we have recently developed a direct real-time target position monitoring method using a gantry-mounted kV/MV imaging system (1, 2) and a gantry-mounted kV imaging system (3). These methods have demonstrated experimental accuracy of <2 mm; however, both methods require continuous kV imaging, resulting in an additional unwanted radiation dose to the patient. Also, the large system latency of 450 ms (1) and 570 ms (3) caused by handling large-size digital kV/MV images reduced the tracking accuracy. One feasible approach to reduce the x-ray imaging dose and latency would be a hybrid position monitoring strategy (4), in which direct stereoscopic x-ray measurement of the internal target position would be supplemented by the external respiratory signals. The respiratory motion would be

Reprint requests to: Byungchul Cho, Ph.D., Department of Radiation Oncology, Asan Medical Center, 86 Asanbyeonwon-gil, Songpa-gu, Seoul 138-736, Korea. Tel: 82-2-3010-4437; Fax: 82-2-482-6987; E-mail: bcho@amc.seoul.kr

Supported by National Cancer Institute Grant R01-CA93626.

Conflict of interest: P. R. Poulsen has received financial support from Varian Medical Systems.

Acknowledgments—The authors are grateful for Varian technical support, particularly Herbert Cattell for the dynamic MLC control program, Hassan Mostafavi and Alexander Sloutsky for sharing their own on-line marker segmentation tool, and Sergey Povzner for the research version of the real-time position management software with dual-output capability to the OBI and the dynamic MLC tracking systems. We also thank Sonja Dieterich for acquiring and preparing the tumor motion database and Libby Roberts for editing the manuscript.

Received Sept 21, 2009, and in revised form Feb 20, 2010. Accepted for publication Feb 22, 2010.

continuously monitored by external surrogates and correlated with the tumor motion, which would be measured using kV/MV imaging. CyberKnife (Accuray, Sunnyvale, CA) has implemented a target tracking scheme by continuously monitoring an external surrogate of the respiratory motion and correlating it with the internal tumor motion measured using kV/kV imaging (4). However, the wide use of this tracking system is limited by the radiosurgery specifications of the CyberKnife. Following a similar rationale, we have developed a hybrid method using gantry-mounted kV/MV imaging and external respiratory monitoring systems that are readily available with conventional treatment machines. With a dynamic multileaf collimator (DMLC) tracking system using this method, the tracking performance was investigated through experiments.

METHODS AND MATERIALS

Real-time target position estimation with DMLC tracking

An external respiratory surrogate, a real-time position management (RPM) system (Varian Medical Systems, Palo Alto, CA), was incorporated into a previously described experimental system (1), in which the target position was measured directly using gantry-mounted kV/MV imaging systems. In the present study, the kV/MV image information was augmented by the external signal and an internal/external correlation model was established to estimate the real-time target position. The target position estimate was fed into a DMLC tracking system to continuously align the beam with the moving target. The integrated DMLC tracking system and the procedure of real-time target position estimation are illustrated in Fig. 1.

The procedure of real-time target position estimation using occasional kV/MV imaging and continuous external respiratory monitoring was as follows (the step numbers refer to those in Fig. 1).

Step 1–3: as described in detail in a previous study (1), the internal target motion, reproduced by a gold marker-embedded phantom on a three-dimensional (3D) motion platform (5), was captured by the kV and MV imaging systems. Immediately after the acquired image was stored on each workstation, a segmentation program extracted the gold marker position from the image and sent it to the DMLC tracking program.

Step 4: once the tracking program had received a kV (or MV) gold marker position, it found the synchronized RPM data based on the measured offset (see the subsequent section, "*Synchronization of kV/MV and RPM data streams*"). The 3D target position was calculated with each kV image by triangulation with the MV images. For each kV image, the MV images acquired immediately before and after it were first used for independent triangulation—these two intermediate triangulation results were then interpolated to minimize the synchronization mismatch between the kV/MV pair.

Step 5: an RPM block was placed on a separate one-dimensional motion platform, which reproduced the external respiratory motion data synchronized with the internal 3D tumor motion. The block was monitored by the RPM system, which fed the optical information to the DMLC tracking program at 30 Hz.

Step 6: the 3D target position from Step 4 and the synchronized RPM data from Step 5 were used to update the correlation model. When new RPM data arrived, the prediction was first applied to compensate for the system latency. Next, the 3D target position was inferred from the predicted RPM data through the correlation model.

Step 7–8: finally, the MLC leaf positions were calculated from the estimated 3D target position and sent to the DMLC controller. The DMLC controller repositioned the MLC leaves to match the updated 3D target position (6).

Synchronization of kV/MV and RPM data streams

The internal target positions from the kV/MV images and external signals from the RPM system experience different delays between the moment of acquisition and their arrival at the DMLC tracking computer. Addressing this discrepancy and accurately synchronizing these elements is essential to building an accurate correlation model. Thus, the following experiment was performed. While the 3D phantom motion of a 2-cm peak-to-peak sinusoidal superoinferior (SI) motion with 20-s period was captured by kV/MV imaging, the synchronous one-dimensional motion of a 2-cm peak-to-peak sinusoidal anteroposterior motion was monitored using the RPM system. By recording the arrival time on the tracking computer for the kV, MV, and RPM data streams using a known input, the relative time offsets for synchronization was measured (*i.e.,* the gold seed positions from the kV [or MV] images and the RPM signals as a function of the arrival time were fit to sinusoidal curves and the time delay of the kV [or MV] image data were calculated from the phase shift of the kV [or MV] fit curve with respect to the RPM curve).

In the present study, we reduced the kV imaging frequency to 1 Hz to demonstrate the reduction of the kV imaging dose to the patient. However, because MV imaging uses the treatment beam without an additional imaging dose cost, it could be used to full capacity. A MV imaging frequency of 5.2 Hz at 200 monitor units (MU)/min was chosen to obtain kV image quality appropriate for marker segmentation, and fluoroscopic kV images were acquired at 1 Hz. One noticeable issue with the OBI imaging system is that an acquired fluoroscopic image is not stored until the next image in the series has been taken. Thus, the time delay from acquisition to triangulation will always be larger than the kV imaging interval. The kV images acquired at 1 Hz were only available for triangulation after 1 s plus the additional time required for image processing and marker extraction. The arrival time of the kV and MV data was delayed 1,088 $\pm$ 37 ms and 263 $\pm$ 28 ms, respectively, compared with the RPM signal. Each kV (or MV) image was synchronized with the RPM data according to this measurement for the correlation model.

Although the large delay of kV data owing to the low imaging frequency delayed the calculation of the target position, it was not critical for real-time tracking because the measured target position was only used for the correlation model. The estimation of the target position itself was updated promptly from the external signal. Hence, the overall latency of the integrated tracking system was only affected by the delay of the RPM data.

Correlation model

For the correlation model (Step 6), we adapted a state-augmented linear method (7) that can implicitly resolve the potential hysteresis between the internal target motion and the external signal. Each motion component of the 3D target position $T(t)$ was continuously estimated by the external respiratory signal $R(t)$ through the correlation model:

$$\begin{pmatrix} T_x \\ T_y \\ T_z \end{pmatrix} = \begin{pmatrix} a_x \\ a_y \\ a_z \end{pmatrix} R(t) + \begin{pmatrix} b_x \\ b_y \\ b_z \end{pmatrix} R(t-\tau) + \begin{pmatrix} c_x \\ c_y \\ c_z \end{pmatrix}$$

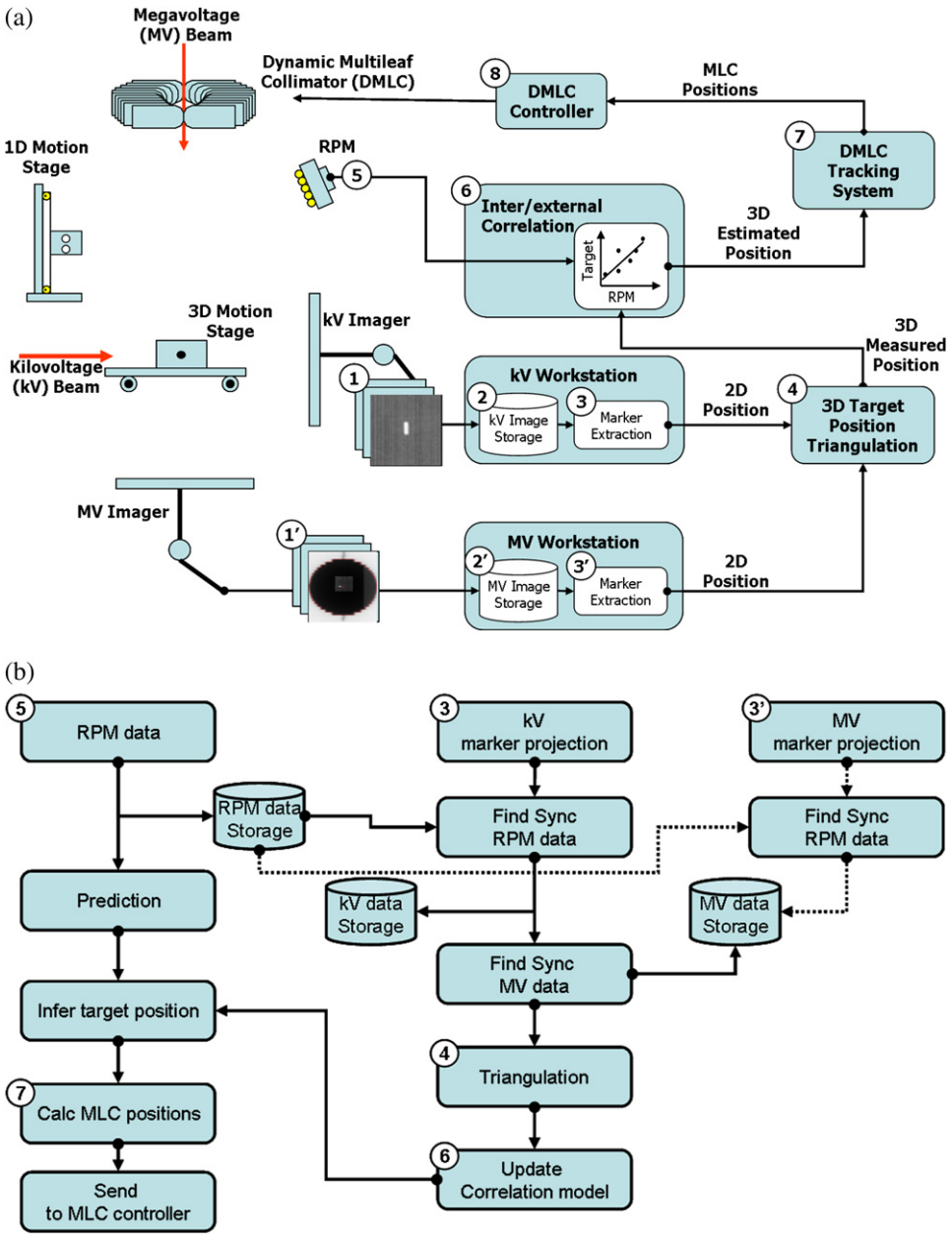

Fig. 1. (a) Overview of integrated dynamic multileaf collimator (DMLC) tracking system and (b) dataflow of kilovoltage (kV)/megavoltage (MV) and real-time position management (RPM) inputs in procedure of real-time target position estimation combining occasional kilovoltage/megavoltage imaging and continuous external respiratory monitoring.

The lag time interval τ needs to be short enough to reflect the local dynamics but also long enough to minimize the effect of noise. τ = 0.5 s was chosen, although the results of the present study were found to be insensitive to this value. The model parameters (a, b, c) can be determined by intermittently acquired target positions $\boldsymbol{T}(t_i)$ using kV/MV imaging and a synchronous external signal $R(t_i)$ using the least-squares estimation (*i.e.,* minimizing the estimation error for each component of the internal target motion):

$$\sum_{i=1}^{N} \|T_x(t_i) - (a_x R(t_i) + b_x R(t-\tau) + c_x)\|^2$$

and similarly for y and z. Here, $N$is the number of synchronized measurements of $\mathrm{T}(t_i)$ and $R(t_i)$ used in the model. The correlation model was first established with N = 5 using the five 3D target positions measured by the same number of kV images acquired. Subsequently, each time a new target position was measured with kV imaging, the model was updated with the latest 15 (if available) target positions.

System latency and prediction

The latency of the entire tracking system was measured by the method described in the previous study (1). The measured delay time was 160 ms, the same as with the previous RPM-alone-based tracking system (8). This value was applied for a linear adaptive filter-based prediction (9) to compensate for the overall system latency.

Tracking experiments

Ten tumor trajectories and associated external respiratory signals with a motion range >10 mm were selected from 160 tumor trajectories (10) acquired from 46 thoracic/abdominal tumor patients treated using a CyberKnife Synchrony system. The beginning 110-s part of each trajectory was used for the tracking experiment, which was composed of the prediction training (40 s) and tracking (60 s) periods. The mean value of the peak-to-peak motion of the selected trajectories was 6.4 mm (range, 1.2–20.8), 13.0 mm (range, 1.0–20.4), and 5.7 mm (range, 1.8–13.7) in the left–right (LR), SI, and anteroposterior directions, respectively. The mean of their average breathing cycles was 3.8 s (range, 2.7–4.9).

Although this method can be used for both static- and rotating-gantry treatment, the entire experiment was performed at a fixed gantry angle such that the MV beam went down vertically and the kV imager was located at the left side of the patient with the patient in a supine head-first position.

The experiment started with the 40-s external respiratory data acquisition for prediction training. During the 40-s prediction training phase, only external respiratory data (in our case, the RPM signal) were acquired. After the prediction was enabled, kV/MV imaging started with MV beam on. Because the correlation model was initialized with five 3D target position measurements, the actual reposition of the MLC leaves began 6 s after the MV beam started. DMLC

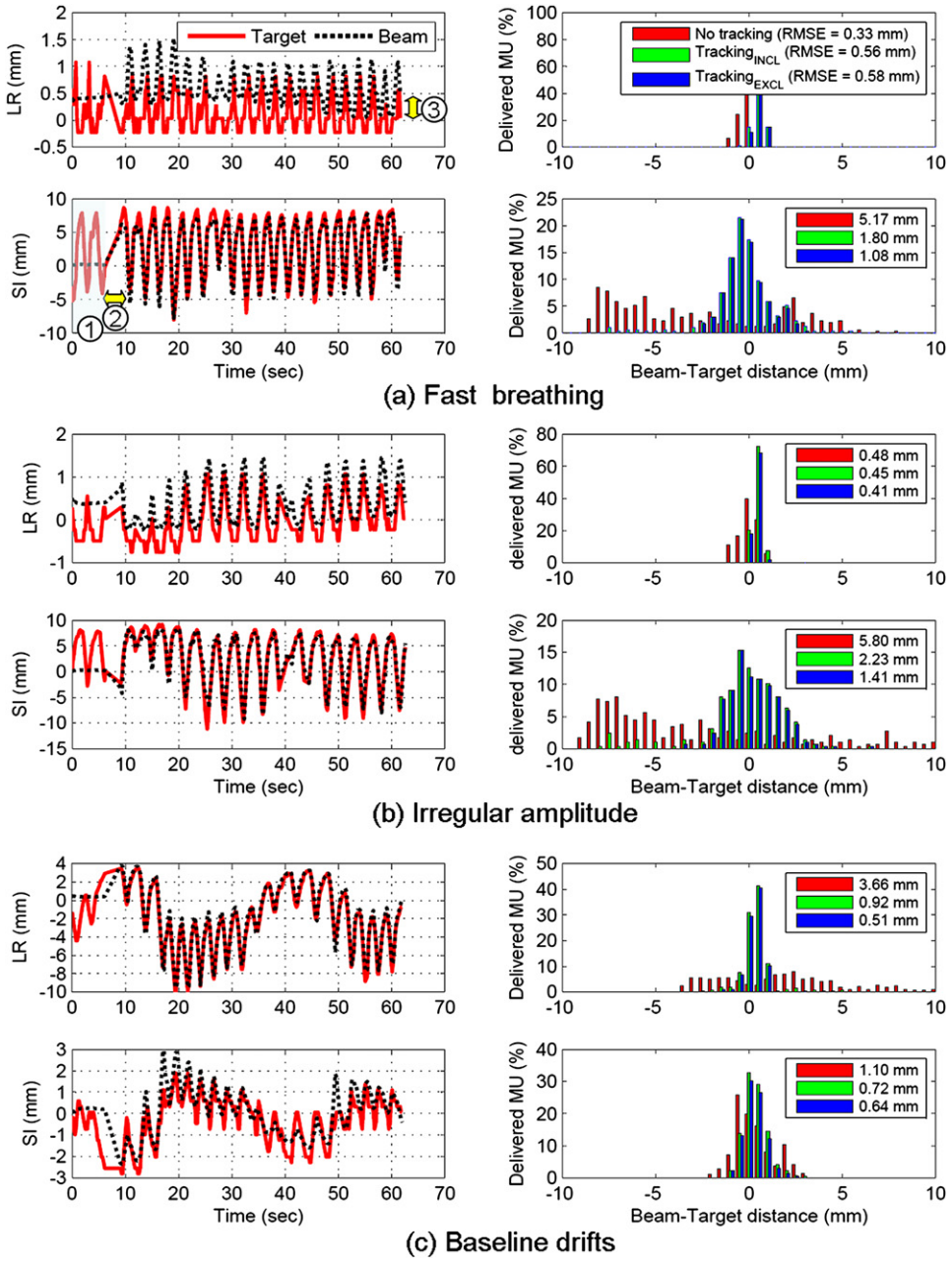

Fig. 2. Beam–target alignment accuracy for three tracking examples: (a) fast breathing motion, (b) irregular amplitude, and (c) baseline drifts. Left–right (LR) and superoinferior (SI) positions measured from megavoltage (MV) beam isocenter on MV imager. RMSE = root-mean-square error. Note that (1) no tracking period of 6 s occurred after MV beam started owing to model building period. It was followed by (2) a beam hold period of 3 s owing to the >5 mm positional difference between the set and actual leaf positions. (3) Systematic shift of 0.4 mm in LR direction reflects machine accuracy of MV beam isocenter. Tracking$_{INCL}$ (or Tracking$_{EXCL}$) indicates tracking accuracy including (or excluding) model building period.

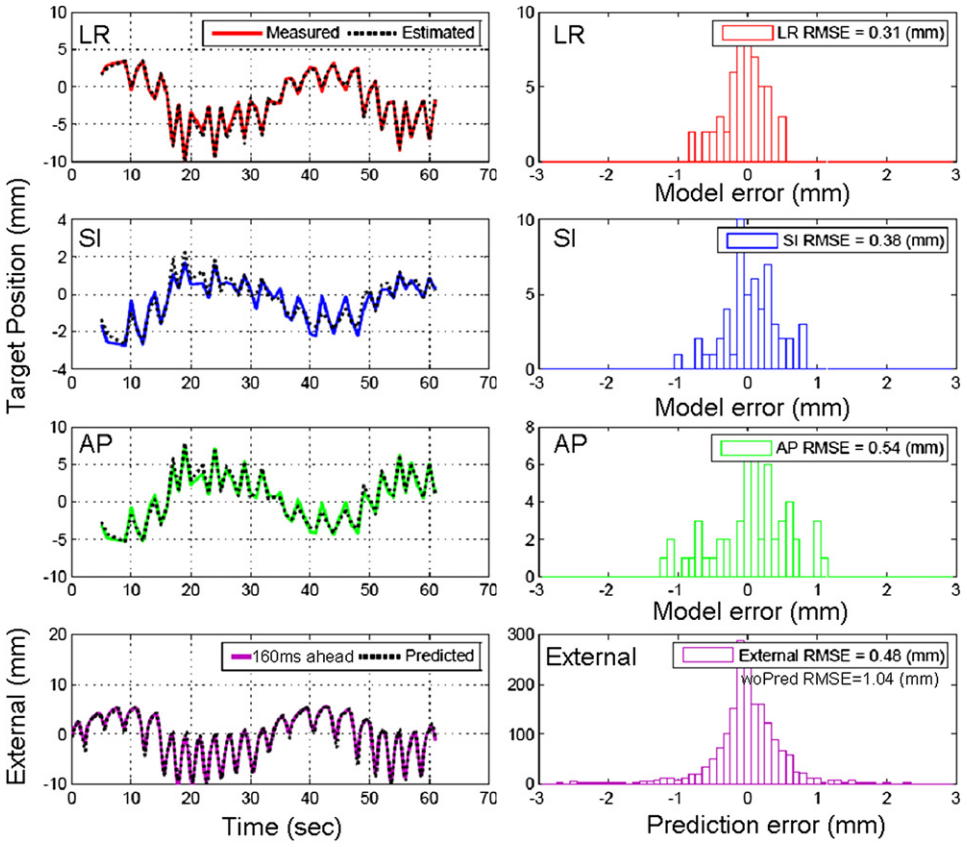

Fig. 3. Example of correlation model and prediction error for Fig. 2c. Upper three rows represent correlation model error in each direction, which measures difference between measured and estimated target positions. Bottom row corresponds to prediction error, which measures difference between predicted and actual input of 160 ms ahead.

tracking with 6 MV and a circular MLC aperture 10 cm in diameter continued for 1 min, until delivering 200 MU at the dose rate of 200 MU/min. With this dose rate, MV imaging was acquired with 0.69 MU/image at the rate of 5.2 Hz (or, equivalently, a 192- ms imaging interval). For each trajectory, the collimator angle was set such that the MLC leaf travel direction matched the major motion direction in either the SI or LR direction.

To investigate the tracking performance, the following data analyses were done for each tracking experiment:

1. The beam–target alignment error (*i.e.,* the beam alignment accuracy to the target position on beam's eye view) was quantified as the distance between the marker position and the center of a circular MLC aperture in each direction on all MV images.

2. Each time the correlation model was updated by a new triangulated target position, the estimated target position using the updated model was recorded. The correlation model error was quantified by the difference between the triangulated and estimated target position for each motion component.

3. The actual external respiratory input and the predicted data were recorded during the tracking experiments. The prediction error was quantified as the difference between the predicted external position and the corresponding actual input that was acquired 160 ms later to account for the system latency.

4. Each time external data arrived, the prediction was applied and the target position was estimated using the correlation model with the predicted external data and the lag external data. The estimated 3D target positions were recorded and compared with the platform trajectory input. The target position estimation error was quantified by the discrepancy between the estimated and the platform input target positions. Although the correlation model error did not include the error contribution from prediction, the target position estimation error was the combination of the correlation model and prediction error.

RESULTS

Figure 2 shows examples of the beam–target alignment errors measured as the positional differences between the target and beam center on the MV images. Regardless of fast breathing motion, irregularities in amplitude, or baseline drift, DMLC tracking with the proposed target positioning method compensated for such target motions effectively. As shown by the histograms in Fig. 2, the errors without tracking were distributed broadly over the motion range and tended to have peaks at the end of the range, which can be expected from the probability density function of the respiratory motion. These error distributions become narrower and close to Gaussian distribution with tracking. The trajectory of the beam showed that the MLC aperture began to follow the target motion˜6 s after the MV beam started and caused a large tracking error. During this period, five kV images were acquired at 1-s intervals and then used for the initialization of the correlation model. A systematic shift between the target and beam positions in the lateral direction was still within the machine accuracy of the MV beam isocenter (0.5 mm) stated by the manufacturer. It could be

further improved by calibrating and correcting the MV beam isocenter according to the gantry and collimator rotation.

Right after tracking started, a beam hold was often asserted by the MLC controller when the difference between the set leaf position by the DMLC tracking system and the actual leaf position was beyond tolerance, which was 5 mm in our experiment. Tracking was resumed ~3 s later when the MLC caught up with the target motion.

Figure 3 shows a typical example of the correlation model error and the prediction error. The correlation model error was submillimeter in all directions and resulted from the inherently incomplete linear correlation between the target motion and the external signal. Other external sources of error contributions would include the external signal noise and the imperfect synchronization between external signal and kV and MV data.

Synchrony tumor trajectory data were not measured directly from the dual kV imaging system but were driven by an external signal through a correlation model similar to the method used in the present study (4). Thus, the tumor trajectory used in the present study was likely to correlate better with the external signal than with the expectation from the real situation; therefore, the correlation model error would have been underestimated. We had previously addressed this issue and assessed the variation of the model-driven estimated position from the measured target position using the Synchrony log files (11). The population mean of the root-mean-square error (RMSE) distributions in three dimensions was 1.5 ± 0.8 mm, which could be converted to 0.8 mm in each direction, assuming the error was distributed evenly in all directions. This result agreed with those from a recent study (12) that used the same method and found that the mean correlation model error was 0.4, 0.8, and 0.8 mm for the LR, SI, and anteroposterior directions, respectively. This suggests that the actual correlation model error would be increased to this amount.

For the 10 experiments, the prediction reduced >50% of the error that might be caused by system latency without prediction. The prediction performance showed that it was not sensitive to the motion range of the external signal or irregularities in amplitude, phase, and baseline.

Figure 4 shows the target position estimation error that was caused both by contributions from the correlation model and prediction errors shown in Fig. 3. The estimated positions were used to reposition the MLC leaf positions.

Figure 5 shows the overall tracking accuracy for the 10 experimental trajectories. Tracking reduced the beam–target alignment error substantially compared with no tracking. The beam–target alignment error with no tracking is likely to be proportional to the range of the motion. In contrast, the beam–target alignment error with tracking was not. The RMSE in the beam–target alignment error, including the model building time period, was <2.5 mm for 1-min tracking. As the tracking time increased, these values would converge

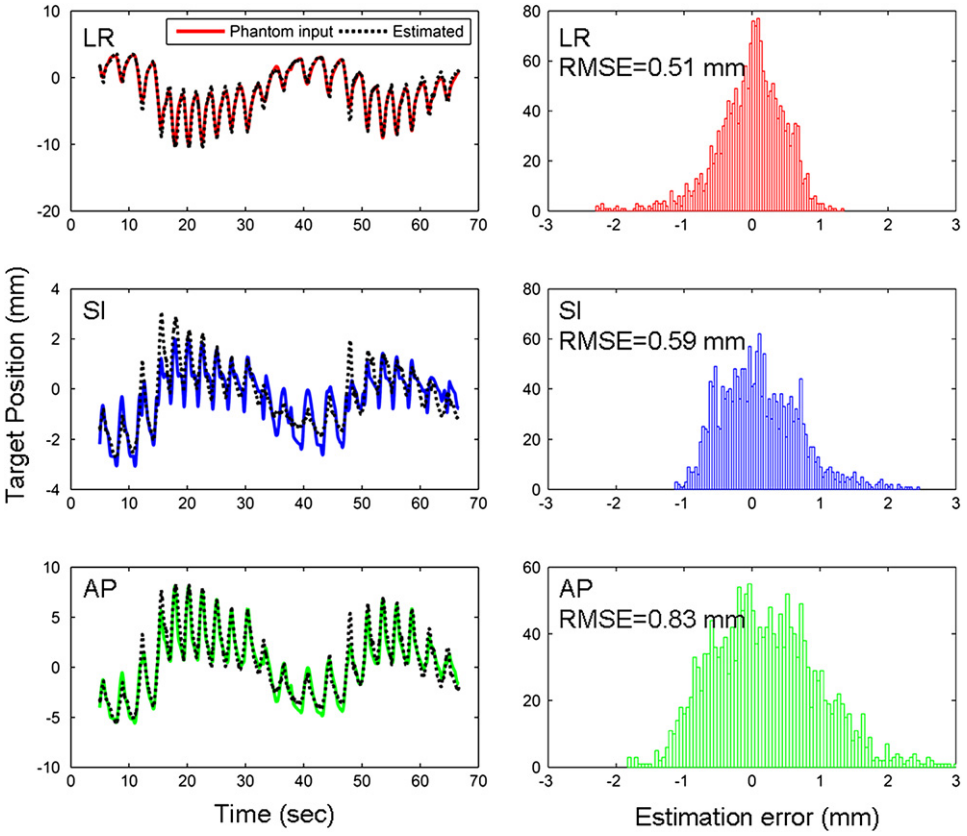

Fig. 4. Example of target position estimation error for same trajectory in Fig. 2c. Scales of y-axis in each direction are different to better illustrate the result.

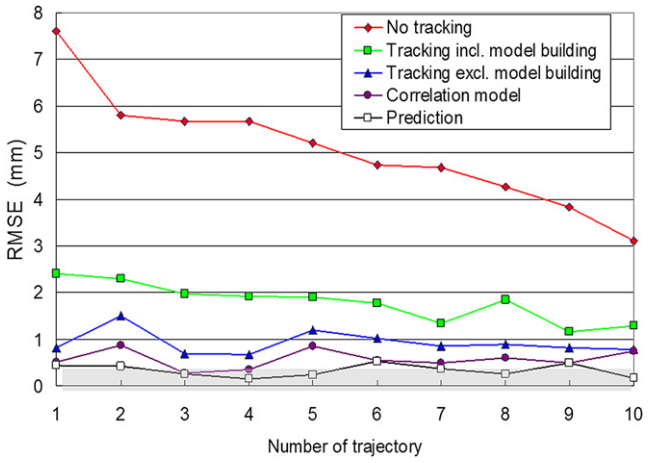

Fig. 5. Beam–target alignment error with and without tracking for 10 experimental trajectories. Gray region represents 0.5-mm machine accuracy of megavoltage beam isocenter specified by manufacturer. Correlation model error and prediction error demonstrated their accuracies were comparable to machine accuracy.

to <1.5 mm, corresponding to the error excluding the model building interval. The error contributions from the correlation model and the prediction are also presented in Fig. 5 for comparison. The RMSE of the prediction error (one-dimensional) was <0.5 mm and the RMSE of the correlation model error (two-dimensional) matched with the beam–target alignment error, which was slightly greater but still <1 mm. The correlation model error and the prediction error demonstrated that their accuracies were comparable to the machine accuracy.

DISCUSSION

The present study has demonstrated that real-time DMLC tracking with target position input using data streams from kV/MV imaging systems and an external respiratory monitoring system, all already available from clinical treatment machines. By establishing an internal/external correlation model and updating it with occasional kV/MV imaging, we obtained accurate estimations of the real-time target position from the external respiratory signals. The benefits of using the proposed hybrid method were the reduction of the kV imaging dose and system latency.

Similar to our previous study, we only used an open aperture to prevent occlusion of the fiducial marker by the MLC leaf and also to measure the tracking error directly using the MV images. The simple MLC aperture and phantom geometry were used in the present study. In practice, however, more complex plans/delivery schemes such as intensity-modulated radiotherapy could have very limited MLC apertures, resulting in occluded marker observations on the MV images. This practical consideration poses a challenge for direct application of the proposed strategy. The use of multiple markers, a marker visibility-constrained intensity-modulated radiotherapy plan (13), or a monoscopic estimation using a kV imager alone (11) are potential solutions to address such concerns. In addition, the fiducial marker segmentation on the clinical x-ray images (especially MV images) is likely to be much more difficult owing to poor contrast or interference with patient anatomy. The development of a robust and reliable marker segmentation method is one of the main challenges to the clinical realization of this method. However, the marker segmentation failure on MV images because

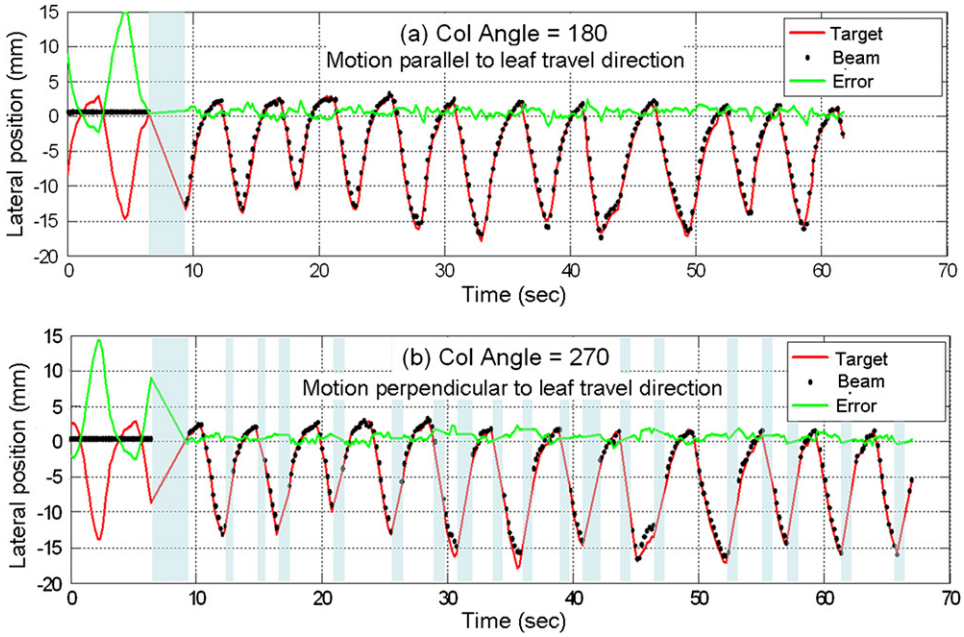

Fig. 6. Comparison of target vs. multileaf collimator (MLC) trajectory of large lateral motion tumor trace for two different collimator angles: (a) collimator at 180° such that lateral motion matched leaf travel direction; and (b) collimator angle of 270° in which lateral motion was perpendicular to leaf travel direction. Gray-shaded periods represent beam-hold intervals caused by leaf speed limitation.

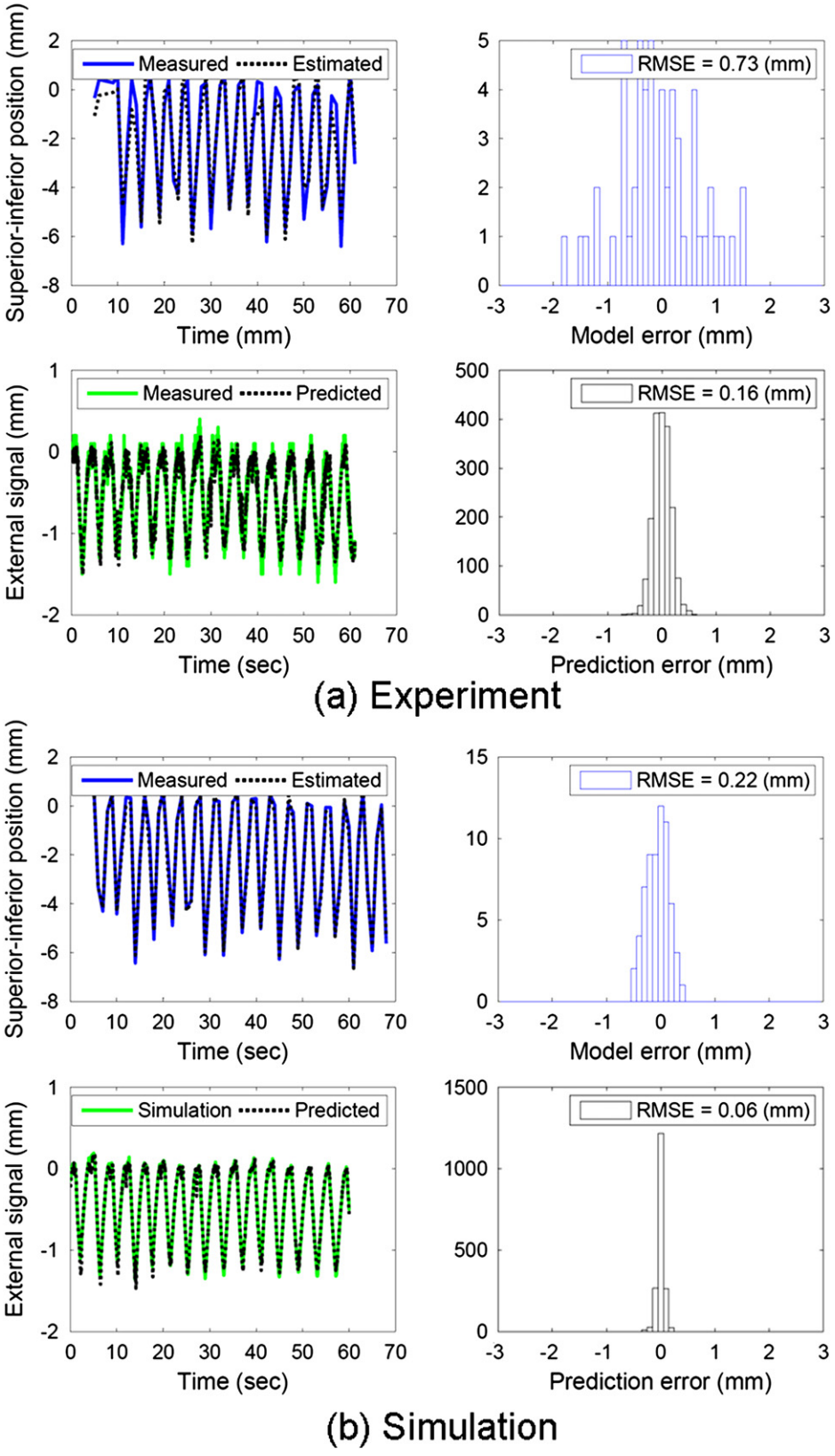

Fig. 7. Experimental results with external signal noise vs. simulation results without external signal noise.

of such complications might not reduce the tracking accuracy significantly, unless the internal/external correlation could change rapidly during the treatment time. This idea has been supported by a recent study using the Synchrony system, which achieved accurate tracking accuracy with the model update every 1 min or several minutes (12).

The potential approaches to reduce the MV beam dose required for correlation model initialization before tracking include decreasing the MV beam dose rate and/or increasing the kV imaging frequency to shorten this interval. Alternatively, pretreatment kV imaging could be used to build the correlation model for at least two motion components, reducing the tracking error significantly during the model setup period. An even more sophisticated method is to build the correlation model using rotational kV imaging alone (14). This initialization procedure was needed only for the first treatment beam; the established correlation model could be used for the following treatment beams without reinitialization, even with a pause between the beams.

To test the effect of the beam hold asserted by the leaf speed limit (15) on the tracking accuracy, the tracking experiments were repeated with two different collimator angles for one trajectory with large LR motion. As shown in Fig. 6, because the trajectory has large LR motion, *(1)* a collimator at 180° such that the LR motion matched the leaf travel direction; and *(2)* for a collimator angle of 270° in which the LR motion is perpendicular to the leaf travel direction, it shows frequent beam holds on mid-inhale or exhale, where the target moves fast perpendicular to the leaf travel direction. Consequently, even though the delivery time was increased by 10%, the tracking accuracy was similar. However, additional reduction of the tracking efficiency would be expected because the shape of the treatment field becomes more complex.

Another interesting finding was the effect of external signal noise. Owing to the linear relationship in the correlation model between target motion and the external signal, the external signal noise would directly affect the position estimation accuracy, especially for patients with small external breathing motion relative to the internal tumor motion. In general, the motion range of the external signals had a similar magnitude of that of tumor motion. However, if the external signal was several times smaller than the tumor motion, the external signal noise directly reinforced the target motion estimation error. Figure 7 shows one example from the tracking experiment demonstrating the effect of external signal noise on the position estimation. Compared with simulation without external noise, experimental data showed noise of standard deviation of 0.1 mm. Because the range of the SI target motion was five times larger than the external signal, 0.1 mm of external noise manifested the error in target position estimation from 0.2 to 0.7 mm. It suggests more accurate respiratory surrogates would be preferable such as a stereo-infrared camera (16) or a stereo-surface imaging system (17).

Finally, although we demonstrated the application of the proposed target position estimation method for DMLC tracking, the method could be more easily applicable to gated radiotherapy, which is being used in the clinic. Because in gated radiotherapy, the external breathing signal alone is often used for target position estimation, the inter- and intrafractional variation of the relationship between the external signal and the internal tumor position could reduce the accuracy (18). With the proposed method, in which the external breathing signal can be supplemented by the intermittent x-ray measurement of the internal target position, the accuracy of gated radiotherapy might be significantly improved.

CONCLUSION

A novel real-time target position estimation method was developed and integrated into a DMLC tracking system. Experimental demonstrations of the integrated tracking system have shown that the geometric error caused by respiratory motion was substantially reduced with the application of respiratory motion tracking. The method used hardware tools available on linear accelerators and therefore shows promise for clinical implementation. However, to overcome the remaining challenges such as the high risk of complications in marker implantation, difficulties in marker segmentation owing to marker occlusion in intensity-modulated radiotherapy fields, and the limited image quality, it requires continuing research and development to yield a robust clinical implementation of this approach. We will continue to study the clinical implication of the challenges and will continue to develop and validate the clinical implementation of the proposed approach.

REFERENCES

1. Cho B, Poulsen PR, Sloutsky A, *et al*. First Demonstration of combined kV/MV image-guided real-time dynamic multileaf-collimator target tracking. *Int J Radiat Oncol Biol Phys* 2009; 74:859–867.
2. Wiersma RD, Mao WH, Xing L. Combined kV and MV imaging for real-time tracking of implanted fiducial markers. *Med Phys* 2008;35:1191–1198.
3. Poulsen PR, Cho B, Ruan D, *et al*. Dynamic MLC tracking of respiratory target motion based on a single kilovoltage imager during arc radiotherapy. *Int J Radiat Oncol Biol Phys* 2009; 74:868–875.
4. Schweikard A, Shiomi H, Adler J. Respiration tracking in radiosurgery. *Med Phys* 2004;31:2738–2741.
5. Malinowski K, Lechleiter K, Hubenschmidt J, *et al*. Use of the 4D phantom to test real-time targeted radiation therapy device accuracy. *Med Phys* 2007;34. 2611–2611.
6. Sawant A, Venkat R, Srivastava V, *et al*. Management of three-dimensional intrafraction motion through real-time DMLC tracking. *Med Phys* 2008;35:2050–2061.
7. Ruan D, Fessler JA, Balter JM, *et al*. Inference of hysteretic respiratory tumor motion from external surrogates: A state augmentation approach. *Phys Med Biol* 2008;53:2923–2936.
8. Keall PJ, Cattell H, Pokhrel D, *et al*. Geometric accuracy of a real-time target tracking system with dynamic multileaf collimator tracking system. *Int J Radiat Oncol Biol Phys* 2006;65: 1579–1584.
9. Srivastava V, Keall P, Sawant A, *et al*. Accurate prediction of intra-fraction motion using a modified linear adaptive filter. *Med Phys* 2007;34:2546–2546.
10. Suh Y, Dieterich S, Cho B, *et al*. An analysis of thoracic and abdominal tumour motion for stereotactic body radiotherapy patients. *Phys Med Biol* 2008;53:3623–3640.

11. Cho BC, Suh YL, Dieterich S, *et al*. A monoscopic method for real-time tumour tracking using combined occasional x-ray imaging and continuous respiratory monitoring. *Phys Med Biol* 2008;53:2837–2855.
12. Hoogeman M, Prevost JB, Nuyttens J, *et al*. Clinical accuracy of the respiratory tumor tracking system of the Cyberknife: Assessment by analysis of log files. *Int J Radiat Oncol Biol Phys* 2009;74:297–303.
13. Ma YZ, Lee L, Keshet O, *et al*. Four-dimensional inverse treatment planning with inclusion of implanted fiducials in IMRT segmented fields. *Med Phys* 2009;36:2215–2221.
14. Cho B, Poulsen P, Ruan D, *et al*. DMLC Tracking with real-time target position estimation combining a single kV imager and an optical respiratory monitoring system. *Int J Radiat Oncol Biol Phys* 2009. Suppl:ASTRO2009 presentation.
15. Wijesooriya K, Bartee C, Siebers JV, *et al*. Determination of maximum leaf velocity and acceleration of a dynamic multileaf collimator: Implications for 4D radiotherapy. *Med Phys* 2005; 32:932–941.
16. Willoughby TR, Forbes AR, Buchholz D, *et al*. Evaluation of an infrared camera and x-ray system using implanted fiducials in patients with lung tumors for gated radiation therapy. *Int J Radiat Oncol Biol Phys* 2006;66:568–575.
17. Bert C, Metheany KG, Doppke K, *et al*. A phantom evaluation of a stereo-vision surface imaging system for radiotherapy patient setup. *Med Phys* 2005;32:2753–2762.
18. Korreman SS, Juhler-Nottrup T, Boyer AL. Respiratory gated beam delivery cannot facilitate margin reduction, unless combined with respiratory correlated image guidance. *Radiother Oncol* 2008;86:61–68.